Lattice curvature generation in graded $In_xGa_{1-x}As/GaAs$ buffer layers

M. Natali*
INFM at the Physics Department, University of Padova, via Marzolo 8, 35131-I Padova, Italy

F. Romanato
INFM-TASC at Elettra Synchrotron, S.S.14 Km 163.5, 34012 Basovizza Trieste, Italy

E. Napolitani, D. De Salvador, and A. V. Drigo
INFM at the Physics Department, University of Padova, via Marzolo 8, 35131-I Padova, Italy
(Received 21 January 2000)

Position dependent lattice tilts in InGaAs/GaAs(001) compositionally graded buffer layers are investigated. The lateral dependence of the tilt defines a concave buffer layer curvature of up to 3 deg cm^{-1}. The buffer layer curvature is associated with a distribution of the misfit dislocation Burgers vectors that varies nearly linearly across the sample. The origin of this peculiar distribution is discussed and is explained in terms of a Burgers-vector selection rule, which governs the cross slip of gliding threading dislocations and that has been experimentally observed by Capano in Phys. Rev. B **45**, 11 768 (1992). A quantitative model of lattice curvature formation is presented that satisfactorily accounts for the main features of the observed buffer layer curvature.

I. INTRODUCTION

Dislocations have ever represented a fascinating topic for materials science, very interesting not only for the basic issue they involve but also for the mechanical modification they induce on materials. Today one of the technologically most relevant applications of dislocations is related to the realization of pseudosubstrates with tunable surface lattice parameter, intended for the integration of optoelectronic heterostructure devices on a single wafer. Such pseudosubstrates are obtained by the growth of compositionally graded buffer layers on top of commercially available substrates. In compositionally graded buffer layers misfit dislocations (MD) are distributed among several low mismatch interfaces, thereby allowing to obtain efficient strain relaxation together with a low threading dislocation (TD) density.[1,2]

In this paper we will focus on an unexpected dislocation distribution in compositionally graded $In_xGa_{1-x}As$ buffer layers grown on well cut (001) GaAs substrates previously described in Ref. 3. The phenomenon consists in a lateral distribution of the MD Burger vectors (BV) giving rise to position dependent lattice tilts. The lattice tilts define a concave curvature of the (001) buffer layer lattice plane, which is not accompanied by any significant curvature of the substrate. The magnitude of the buffer layer curvature in some cases reaches values up to 3 deg cm^{-1}.

The interest of lattice tilt studies lies in the close relationship between lattice tilts and dislocation generation mechanisms. Lattice mismatched layers grown on substrates, offcut some degrees from the (001) plane, have shown large tilts of the layer lattice with respect to the substrate, aligned parallel to the off-cut direction.[4–9] The origin of these tilts has been attributed to a preferential nucleation of MD's with vertical component of the BV oriented in order to reduce the surface off-cut angle. Models of lattice tilt formation based on this idea have been developed by Ayers *et al.*,[4] by Legoues *et al.*[9] and more recently by Riesz[10]. In particular Legoues *et al.* have been able to deduce the MD nucleation energy from a comparison between their model prediction with experimental lattice tilt data.

According to the above-mentioned models, in the case of well cut (001) substrates, no tilt formation is expected because of the lack of a BV selective driving force. Nevertheless lattice tilts have been also observed on well cut (001) substrates in Refs. 11–14, suggesting that also on well cut substrates there must exist a driving force for the selection of the BV's. This has been confirmed definitely by the observation of a buffer layer curvature in compositionally graded InGaAs/GaAs(001) buffer layers in Ref. 3.

Here we will give a contribution to a deeper understanding of the lattice tilt formation process by investigating buffer layer curvatures in several compositionally graded InGaAs/GaAs(001) buffer layers. The depth profile of the curvature has been determined by means of x-ray diffraction reciprocal space map measurements performed with synchrotron radiation. Detailed maps of lattice tilts on the buffer layer surface have been obtained by Rutherford backscattering spectrometry measurements performed in channeling condition. We present a quantitative model of lattice curvature formation based on the Burgers vector selection produced by the cross slip of gliding threading dislocations,[15] which occurs in Frank-Read and spiral dislocation multiplication mechanisms.[15–18] The model satisfactorily accounts for the main features of the buffer layer curvature.

II. EXPERIMENT

Graded InGaAs buffer layers with different composition profiles were grown by solid source molecular beam epitaxy at a temperature of 500 °C on semi-insulating liquid-encapsulated Czochralski GaAs(001) substrates. The substrate surface was (001) oriented to an accuracy of 0.1 deg. The samples we consider have a composition profile graded

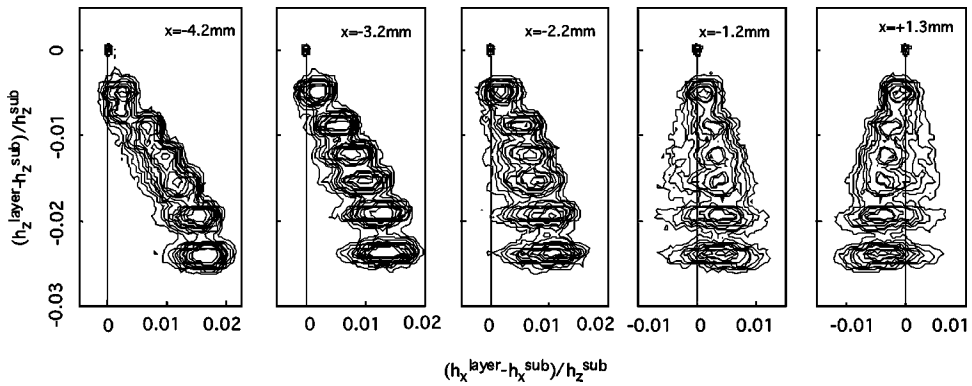

FIG. 1. (004) reciprocal space maps collected at different positions on the surface of a InGaAs/GaAs buffer layer with a steplike composition profile having six composition steps (sample ST6). The spatial coordinates refer to the frame of reference, $x=[110]$, $y=[\bar{1}10]$, and $z=[001]$. From left to right: $x=-4.2$ mm, -3.2 mm, -2.2 mm, -1.2 mm, $+1.3$ mm ($y=0$ mm). The ordinate and abscissa represent normalized reciprocal space coordinates referred to the substrate peak and give, respectively, the lattice tilt in radians and the lattice mismatch along the z direction. The lattice tilt increase with increasing lattice mismatch of the layer. For a given layer the tilt changes with the position on the sample.

following both steplike or continuous depth profiles. In the case of step-graded buffer layers the total thickness and the surface indium composition have been nominally divided in 3, 6, and 9 equal composition steps (samples ST3, ST6, and ST9). The continuously graded buffer layers have been designed following three types of composition profiles: linear, square root, and parabolic with the maximum composition at the surface. For all the profiles the nominal total thickness was $t_b=2300$ nm and the surface composition $x_b=0.35$. The substrates had dimensions of 16×13 mm^2 and were kept in rotation during the growth to avoid composition disuniformities. Other details of the growth procedure are reported in Ref. 19.

X-ray diffraction (XRD) measurements were performed with a triple-axis diffractometer at the beam-line BM05 of the European Synchrotron Radiation Facility ESRF (Grenoble, France) by using a wavelength of 1.499 Å. The beam spot had a footprint on the sample surface of 1×1 mm^2 for all the measurements. The indium composition and relaxed misfit were determined by collecting maps around the (004) and (335) points of the reciprocal space and by analyzing the data according to standard procedures.[20]

Reciprocal space maps (RSM's) provide an absolute measurement of the tilt because they give the position of the step-layer diffraction peaks relative to the substrate peak. RSM's were collected scanning the surface typically with a 4-mm-step network.

To determine the total thickness and the indium composition profile of the buffer layers Rutherford backscattering spectrometry (RBS) was carried out with 2 MeV and 4 MeV $^4He^+$ ions, delivered by Van de Graaff accelerators of the Laboratori Nazionali di Legnaro (Italy). The composition was cross checked with the determination provided by RSM's.

The tilt analysis was also performed by RBS channeling measurements using a triple-axis goniometer with an accuracy of the rotations of 0.01 deg. The rather quick data acquisition ($2-3$ min/point) and analysis allows us to obtain detailed surface tilt maps with a lateral resolution of 0.5 mm corresponding to the beam-spot dimension.

Although the RBS-channeling technique can probe a thickness of several microns, the channeling analysis of the tilt is limited to the topmost region of the epilayer (≈100 nm). In fact, the trajectories of the channeled ions are steered and therefore constrained to follow the depth evolution of the epilayer deformation. As a consequence one cannot measure the lattice orientation of the deeper regions.[21] Moreover the signal from the substrate cannot be used as a reference and an arbitrary reference direction has been chosen for the channeling maps. The absolute lattice tilt at a reference point has been measured by means of XRD and it was used to calibrate the RBS-channeling determination of lattice orientations, hence obtaining a map of absolute surface lattice tilts referred to the substrate.

III. RESULTS

Typical (004) RSM's, recorded at different positions on the sample surface, are shown in Figs. 1 and 2 for buffers ST6 and ST9, respectively. The peaks of the substrate and of the layers are clearly separated. The spatial coordinates refer to the following Cartesian frame of reference: $x=[110]$, $y=[\bar{1}10]$ lying in the (001) surface plane and $z=[001]$ the surface normal. The origin of the (x,y) coordinates is chosen at the sample center. The ordinate and abscissa in Figs. 1 and 2 are normalized reciprocal space coordinates. h_i^{layer} and

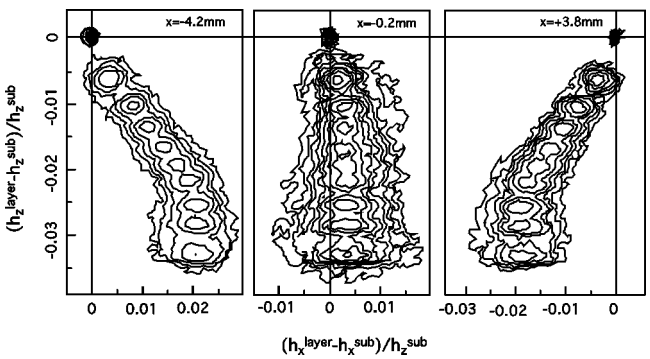

FIG. 2. (004) reciprocal space maps collected at different positions on the surface of a nine-step buffer layer (sample ST9). From left to right $x=-4.2$ mm, -0.2 mm, and $+3.8$ mm ($y=0$ mm).

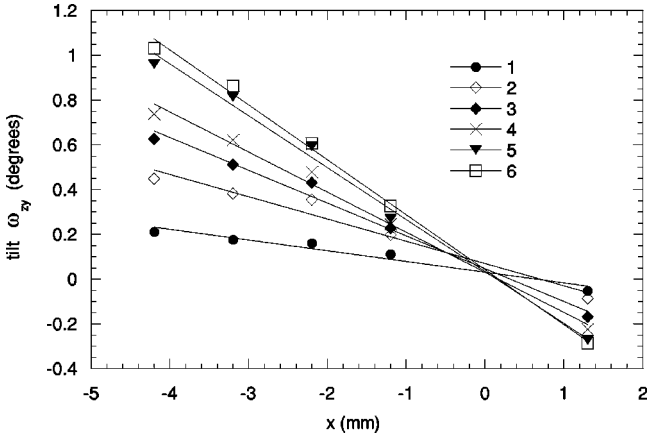

FIG. 3. Lateral dependence of the film tilt ω_{zy} as a function of the x coordinate as measured by the reciprocal space maps of Fig. 1. The data points can be well fitted by straight lines

h_i^{sub} (with $i=x,y,z$) are the reciprocal space coordinates along the i direction of the layer and substrate, respectively. For the substrate (004) Bragg reflection $h_x^{sub}=h_y^{sub}=0$ and $h_z^{sub}=2\pi/4a$, where a is the GaAs lattice parameter. While the ordinate $(h_x^{layer}-h_x^{sub})/h_z^{sub}$ gives the lattice tilt of the layer in radians, the abscissa $(h_z^{layer}-h_z^{sub})/h_z^{sub}$ represents the layer-substrate lattice mismatch perpendicular to the layer surface.

The lattice tilt of the layers increases with increasing perpendicular lattice mismatch, i.e., as we consider layers lying nearer to the surface. For buffer ST9 we observe also a saturation of the lattice tilts in the last two layers. However, the most important feature is that the lattice tilt of a given layer changes as we consider different points on the sample surface. The lateral dependence of the lattice tilt as a function of the x coordinate at $y=0$ is shown in Figs. 3 and 4 for buffer ST6 and buffer ST9, respectively. Here we have indicated by ω_{zy} the rotation of the layer z axis around the y axis. Similarly we will indicate by ω_{zx} the layer z axis rotation around the x axis.

The lateral dependence of the tilt is almost linear for all

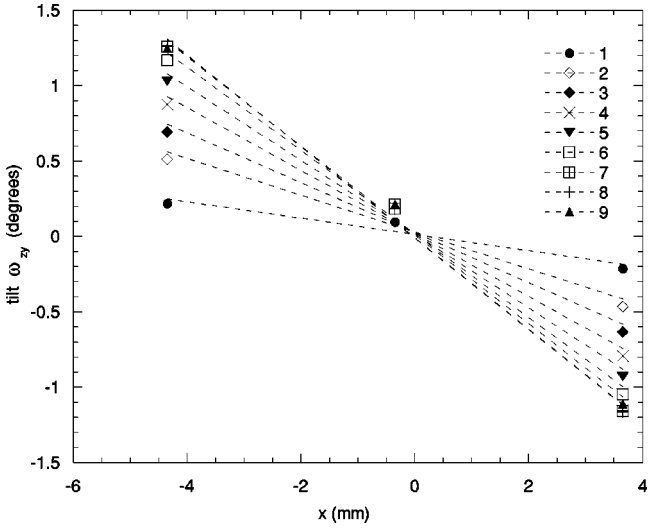

FIG. 4. Lateral dependence of the film tilt ω_{zy} as a function of the x coordinate as measured by the reciprocal space maps of Fig. 2.

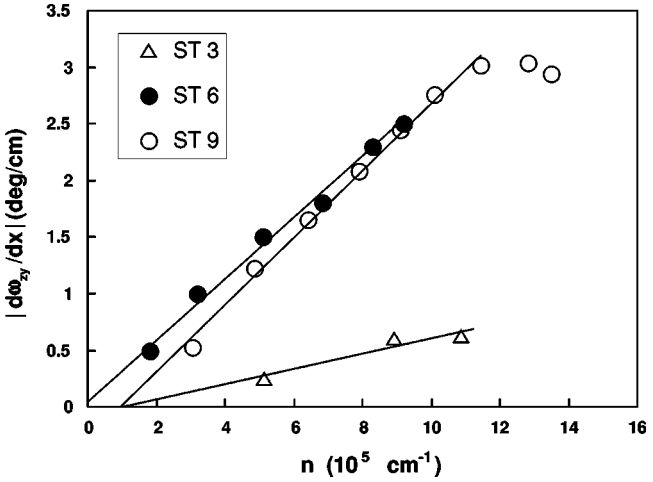

FIG. 5. The average curvature of the lth layer is shown as a function of the MD density integrated from the first up to the lth interface. Open circles represent data from sample ST9, full circles from sample ST6, and triangles from sample ST3.

the layers and so defines a constant curvature for each of the layers. The curvature starts at the film-substrate interface and increases towards the sample surface. The slope of the lines provides a measure of the average curvature. The negative slope corresponds to a *concave* curvature of the layer (001) planes if the sample surface is viewed from the top.

Concerning the thickness dependence of the curvature it is important to underline that in the substrate there is no significant curvature. By measuring the substrate peak angle in XRD rocking curves as a function of the position on the sample, the substrate curvature was estimated to be $\leqslant 0.1$ deg cm^{-1} for all the samples. This fact is noteworthy because it implies that the curvature develops only in the film region.

It is well known that strain relaxation in InGaAs/GaAs layers occurs mainly by the formation of 60^0 MD's with a/2 $\langle 110\rangle$ BV. Then the MD density at each of the interfaces of the step-graded buffer layers can be determined from the XRD measurement of the lattice mismatch parallel to the interfaces from the relationship $n_i=m_j/b_j$ $(j\neq i)$. Here we have indicated by n_i the density of MD's, parallel to the i direction, at a given interface. m_j is the lattice mismatch parallel to the j direction between the two layers adjacent to the interface under consideration and b_j is the misfit dislocation's BV edge component parallel to the j direction.

In Fig. 5 we report the curvature $\partial\omega_{zy}/\partial x$ of the lth layer as a function of MD density integrated from the first up to the lth layer. The MD density refers to MD's parallel to y. The curvature increases linearly with the MD density over a large interval. The plateau of the curvature at high MD densities for sample ST9 corresponds to the saturation of the lattice tilts in the last two layers observed in the RSM in Fig. 2.

The rate of curvature formation is much higher for buffer ST9 and ST6 than for buffer ST3, indicating a composition profile dependence of the curvature. A further composition profile dependence of the curvature phenomenon is evident from Table I where we report the curvature of buffer layers with different step and continuously graded composition profiles. It is worth to note that where available the channeling

TABLE I. The surface curvature as determined from RBS channeling and XRD (+) are reported in columns 2 and 3, the average MD density is given in column 4, and the BV alignment parameter k in column 5 for buffer layers with different composition profiles. For steplike profiles k has been calculated from $\partial\omega_{zy}/\partial x$ and for continuous profiles from the average curvature $(\partial\omega_{zy}/\partial x + \partial\omega_{zx}/\partial y)/2$.

Composition profile	$\frac{\partial\omega_{zy}}{\partial x}$ ($^\circ$ cm^{-1})	$\frac{\partial\omega_{zx}}{\partial y}$ ($^\circ$ cm^{-1})	n (10^5 cm^{-1})	k
Steplike				
ST9	$-2.9^{(+)}$ -2.8	-0.04	13.7	0.78
ST6	$-2.4^{(+)}$ -2.5	-0.01	9.2	0.98
ST3	$-0.62^{(+)}$	$-0.2^{(+)}$	10.7	0.22
Continuous				
Linear	-0.8	-0.7	9.3	0.34
Parabolic	-1.0	-0.7	10.3	0.35
Square root	-1.5	-0.9	10.1	0.50

determination is in good agreement with that obtained by RSM's.

An overview of the surface layer tilt distribution measured by RBS channeling is shown in Fig. 6 for sample ST9. The arrows represent the tilt vectors $(\omega_{zy}, \omega_{zx})$ which correspond to the projection of the [001] axis of the buffer layer onto the sample surface. The tilt vectors point towards the sample center and define a concave curvature, i.e., $\partial\omega_{zy}/\partial x < 0$ and $\partial\omega_{zx}/\partial y < 0$. The tilt is approximately null near the sample center. The average surface curvature measured along the x and y directions is given in Table I and is much larger along the x direction than along the y direction. This curvature asymmetry is mainly limited to buffer layers with a step composition profile.

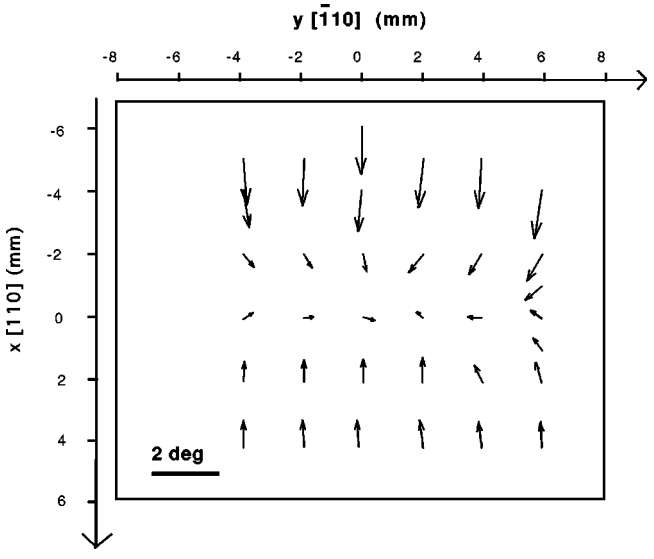

FIG. 6. Schematic representation of the [001]-axis orientation as measured by RBS channeling at different points on the sample surface of buffer ST9. The arrows represent projection of the surface [001] axis onto the (001) interface plane. The x and y components of the arrows give the tilts ω_{zy} and ω_{zx}, respectively. The magnitude of the lattice tilts can be estimated by comparison with the marker.

A feature common to all the samples analyzed, which can be appreciated in the map of surface tilts in Fig. 6, is that the tilt component ω_{zy} is almost constant as we consider measurements at points with constant x coordinate, i.e., $\partial\omega_{zy}/\partial y \approx 0$. Similarly $\partial\omega_{zx}/\partial x \approx 0$.

IV. CURVATURE FORMATION MECHANISM

The observed film curvature cannot be of elastic origin. In fact, an epitaxial layer under compressive strain exerts a tensile stress on the substrate at the layer-substrate interface and therefore induces a *convex* curvature of the whole layer +substrate system. This however is in contradiction with the observed *concave* nature of the curvature that moreover is localized only in the film region.

These features exclude also thermal stress as a cause for the curvature formation. In the latter case the curvature is due to different thermal expansion coefficients of the layer and substrate materials that induce a thermal stress during the cooling down from growth temperature to ambient temperature. In our case the thermal expansion coefficient for InGaAs is smaller than for GaAs. Then the thermal stress that the layers exert on the substrate is again tensile and should therefore induce a *convex* curvature. We thus conclude that the concave buffer layer curvature must be of plastic origin.

The dislocations mainly responsible for the plastic deformation of InGaAs/GaAs buffer layers are $a/2\langle 110\rangle 60^0$ type misfit dislocations. Tilts associated with such MD's are related to the dislocation's BV edge component perpendicular to the interface b_z (see for instance Ref. 22). More specifically, if we indicate by n_{i+} and n_{i-} the densities of MD's that are parallel to the i axis and have positive or negative b_z component, respectively, then the lattice tilt generated by these MD's is given by

$$\omega_{zi} = (n_{i-} - n_{i+})|b_z|. \tag{1}$$

From Eq. (1) it follows that in the case of a uniform imbalance among the MD densities n_{i-} and n_{i+}, a constant lattice tilt is generated. *Vice versa*, from the experimentally observed linear position dependence of the tilts, we conclude that there exists a linear variation of the MD's b_z component

$$<b_z> = k|b_z|\frac{x}{L/2}. \tag{2}$$

Here L is the sample length along the x direction and k is a parameter that measures the BV alignment at the sample border. $<b_z>$ indicates a local average over MD's, performed on a length scale that is much larger than the MD spacing whereas being smaller than the beam-spot diameter used for the RBS and XRD measurements.

Even though we are not able to give a direct microscopic confirmation of the validity of Eq. (2) in the following, we will take its validity for granted. We are encouraged in this respect by the fact that the relationship between lattice tilts in relaxed lattice mismatched layers and the BV's of $a/2\langle 110\rangle 60^0$ type MD's expressed by Eq. (1) is based on a firm ground.[5,8,9]

A positive value of k corresponds to a concave curvature and for $|k| = 1$ all the MD's at the sample border have the

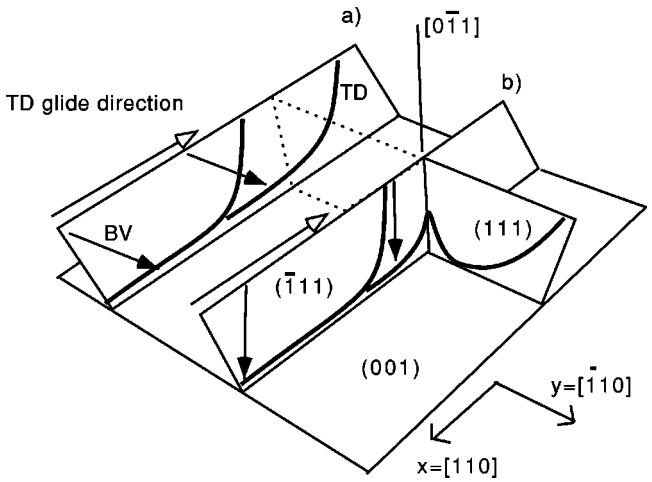

FIG. 7. Two $a/2\langle 110\rangle 60^0$ MD's with the associated gliding TD arms are shown. The TD in (a) has its Burgers vector BV almost perpendicular to the TD arm. The TD in (b) has its BV almost parallel to the TD arm and therefore may undergo cross slip onto a transverse {111} glide plane.

same b_z component. Experimental values of k can be obtained from the relation $k=-(\partial\omega_{zy}/\partial x)/(2n_y|b_z|/L)$. In Table I we report the values of k obtained from the buffer layer surface curvature and the total density of MD's on buffer layers with different composition profiles. The values range from $k=0.22$ for buffer ST3 up to $k=0.98$ for buffer ST6.

This description raises the question how such a BV distribution might arise. To address this question let us analyze the formation and propagation of $a/2\langle 110\rangle$ 60^0 MD's in lattice mismatched layers under compressive stress.

MD's elongate through the glide of an associated threading-dislocation arm that lies on a {111} glide plane (see Fig. 7). It may happen that a gliding threading arm cross slips from a {111} glide plane to a transverse glide plane as shown in Fig. 7(b). This is a process that has been observed in many MD multiplication mechanisms (see for instance Refs. 15–18) as well as independently from MD multiplication in Refs. 23–25.

The cross slip of the TD arm is possible provided that:[26]

(i) part of the TD arm lies on the intersection between the two {111} glide planes, i.e., on an inclined $\langle 110\rangle$ direction,

(ii) the BV is parallel to the TD line direction, i.e., the TD segment is of screw type.

Our model is based on the following observation: gliding TD arms are inclined with respect to the (001) plane and the TD segment is forming an obtuse angle with the MD that lies in the wake of the gliding TD. In other words, TD's are forward pending towards the TD propagation direction. The reason for this behavior lies in the force acting on the TD that tends to maximize the strain relaxation produced by the dislocation compatible with the dislocation line tension. Two groups of gliding TD's, which have very different cross-slip probabilities, can be distinguished: TD's that have their BV nearly perpendicular to the TD arm—an example of this situation is shown in Fig. 7(a)—and TD's whose BV is almost parallel to the TD arm—an example of which is shown in Fig. 7(b). The cross slip probability is much higher for the second set of TD's than for the first.

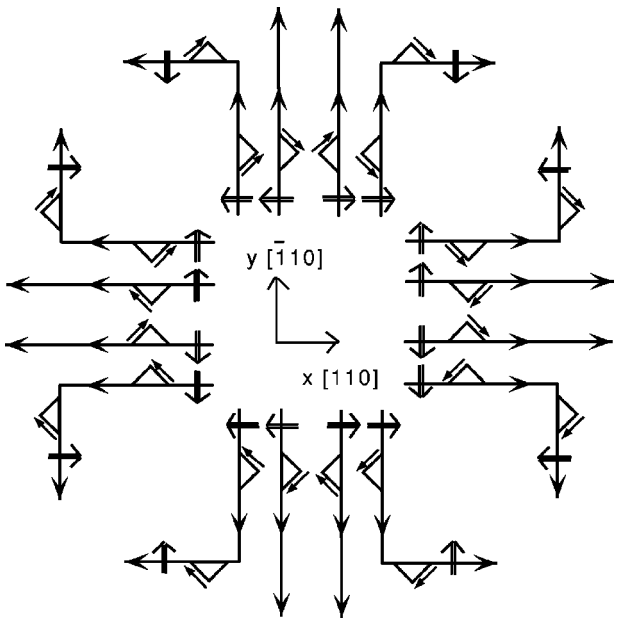

FIG. 8. Schematic [001] top view of the allowed $a/2\langle 110\rangle 60^0$ MD's relaxing strain in a InGaAs layer under compressive stress and of the corresponding allowed cross slip events. The {111} glide plane is shown by a triangle whose base is parallel to the MD line and whose tip points towards the layer surface. The dislocation line directions are chosen to coincide with the TD propagation direction. The Burgers vectors are indicated by arrows that lie on the MD glide plane. The double arrows represent the microscopic lattice tilt vectors $(\omega_{zy},\omega_{zx})$ associated with each MD.

This has indeed been experimentally observed by Capano[15] in SiGe/Si(001) layers. Since the above argument involves only geometric properties, its validity can be extended to the case of InGaAs/GaAs(001) heterostructures. In the following we will refer to the above property as to a *''Burgers vector selection rule.''* The consequences of this BV selection rule turn out to be fundamental for lattice tilt generation. In fact by analyzing the allowed cross slip events for all possible a/2$\langle 110\rangle$ 60^0 MD's, we are led to formulate the following property:

''Lattice tilts related to cross slipped MD's are always directed opposite to the TD propagation direction before cross slip.''

The justification of this property can be obtained by considering the [001] top view of all possible a/2$\langle 110\rangle$ 60^0 MD's that relax the compressive strain present in the InGaAs layer, shown in Fig. 8. To relax the compressive strain, the extra-half plane associated with the MD, must lie in the substrate. This condition is met when the resultant of the vector product $\bar{\zeta}$ x $\bar{b}_{||edge}$ points towards the negative z axis. Here $\bar{\zeta}$ is the conventional dislocation direction and $\bar{b}_{||edge}$ is the BV edge component parallel to the interface. For convenience in Fig. 8 we have chosen $\bar{\zeta}$ equal to the MD/TD propagation direction. The {111} glide plane is indicated by a triangle whose base touches the MD line and whose tip points towards the layer surface. The BV's are indicated by arrows that lie on the glide planes. The double arrows perpendicular to the MD lines represent the direction of the tilt vectors $(\omega_{zy},\omega_{zx},0)$ associated with each MD. The direction of the tilt vectors is given by $\bar{b}_z$ x $\bar{\zeta}$ where $\bar{b}_z=(0,0,b_z)$.

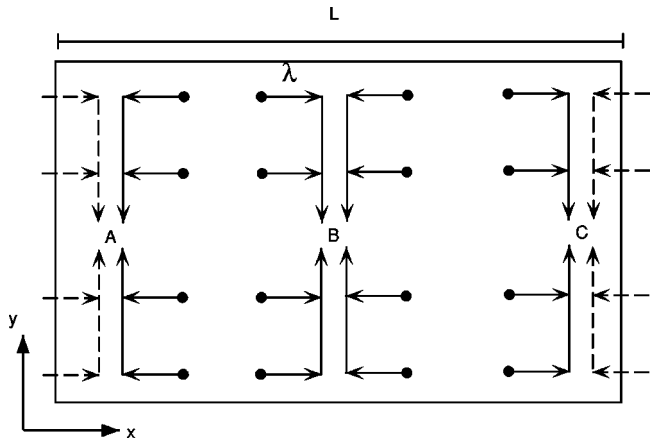

FIG. 9. The cross-slip of TD's originally gliding parallel to the x direction leads to different densities of MD's parallel to the y direction depending on the position on the sample surface: at point A the MD's that have arisen from cross slip of TD's originally propagating towards the negative x axis dominate. The opposite is true for point C. At point B the densities of MD's, which arise from cross slip of TD's originally gliding in opposite directions, are equal. λ indicates the average glide length of MD's before cross slip and L the sample size.

According to the above described BV selection rule, only half of the TD's gliding in a given direction are able to cross slip. The propagation direction of the MD's after cross slip is determined by the condition that the MD's relax the compressive strain in the layer. The inspection of the tilt vectors for the different cases shown in Fig. 8 confirms that they are always directed opposite to the TD propagation direction before cross slip. It is worth noting that this property is independent of the choice of the conventional dislocation direction.

From this property it follows that a net lattice tilt can be generated when there exists an imbalance in the populations of TD's gliding in opposite directions. Such an imbalance actually occurs on any finite-size sample.

To understand this fact let us consider the MD's that reach a given point along the y direction after having undergone cross slip and that generate the ω_{zy} lattice tilt component. In Fig. 9 we consider schematically the situation for MD's that reach a point at the sample center (point B) and two points near opposite sample borders (points A,C). The average glide length of MD's before cross slip occurs is indicated by λ. For point B the number of TD's gliding along the positive and negative x direction are the same for symmetry reasons. Hence there will be no net lattice tilt generation at the sample center.

On the contrary, for the points A,C that we supposed to lie within a distance λ from the nearest sample border, there will be an excess of TD's gliding towards the negative and positive x direction, respectively. The reason is that near the sample border the symmetry is broken because TD sources cannot lie outside the sample area. As a consequence, the imbalance of TD populations generates a net lattice tilt at points A and C. The lattice tilt is positive in A and negative in C. In terms of tilt vectors $(\omega_{zy},0)$, these are directed toward the sample center in agreement with the experimental observations (Fig. 6).

V. COMPUTATION OF THE BUFFER LAYER CURVATURE

In order to calculate the lattice tilt distribution arising from the above described effect, we introduce some approximations.

(i) We assume that the cross-slip probability is null for those dislocations that have their BV almost perpendicular to their gliding TD arm. On the contrary, for the dislocation set with the BV almost parallel to the TD arm, we assume that there is a constant cross slip probability per unit glide length.

If we indicate by λ the average propagation distance of a TD before cross-slip occurs, then we can identify the cross slip probability per unit length with $1/\lambda$. Due to the lack of inversion symmetry of the zinc-blende lattice of InGaAs, the MD's along the x and y directions are not equivalent.[27] The $a/2\langle 110\rangle$ 60^0 MD's parallel to $y=[\bar{1}10]$ in InGaAs/GaAs layers have Group-III core atoms and are called α-MD's. On the other hand, MD's parallel to $x=[110]$ have Group-V core atoms and are called β-MD's. It is now well established that, for InGaAs layers under compressive stress, α-MD's have a lower-activation energy for glide and nucleation than β-MD's.[28] From this it follows that we must distinguish between cross slip glide lengths λ_α and λ_β for TD's gliding, respectively, along the x and y directions.

We are not aware of any measured values of λ. However a direct measurement of the cross slip glide length could be done in the early stage of the relaxation process in low-mismatch InGaAs/GaAs layers by real-time *in situ* x-ray topography as suggested by the work of Lacey *et al.*[24]

(ii) We assume that the glide length of MD's is long enough that all MD's are able to reach the sample border.

This appears a reasonable assumption in the case of InGaAs/GaAs compositionally graded buffer layers since these are especially designed to yield very long dislocation glide lengths. We will discuss this point later.

There are different possible sources generating MD's during the strain relaxation process of a lattice mismatched epitaxial layer. MD's may arise from substrate TD's, may nucleate at the layer surface or at heterogeneous particles, or near substrate surface imperfections. In the following we will call all these sources *extrinsic sources* and indicate by ρ_α and ρ_β the areal densities of such sources that generate α and β-MD's, respectively.

(iii) For MD's generated by extrinsic sources we will assume that the BV's are uniformly distributed among the allowed $\langle 110\rangle$ directions and that extrinsic sources are homogeneously distributed on the sample area.

On the other hand, MD's may be generated by means of various MD multiplication mechanisms, such as the spiral source and the Frank-Read multiplication sources observed in Refs. 15–18. A special property of MD multiplication sources consists in their ability to replicate MD's, which all have the same BV. This is the reason why MD multiplication mechanisms play an important role in relationship with lattice tilt formation models (see for instance Refs. 9 and 10).

The above-mentioned MD multiplication sources all involve the cross slip of gliding TD's and the generation of an array of MD's lying on the transverse (111) glide plane. We may schematically describe these sources within the framework of our model by giving the average number N of MD's

in such arrays. Such arrays have been associated with MD-pileups observed in compositionally graded buffer layers in Refs. 9 and 27. Therefore N may be directly measured.

Capano[15] has given conclusive experimental evidence that such multiplication mechanisms obey the same BV selection rule illustrated above for simple cross slip.

(iv) To keep the calculations sufficiently simple we will assume that the MD's generated in a multiplication source will not further activate new multiplication sources by repeated cross slip. In other words we will neglect MD's resulting from all but the first cross slip in a possible multiple cross-slip sequence. The validity of this choice will be discussed later.

For the calculation of the lattice tilt distribution, let us determine the density of MD's parallel to the y direction, $n_\alpha(x,y)$, at some point (x,y) on a square sample of size $L \times L$. Several terms contribute to this density. A first contribution comes from extrinsic sources of α-MD's that are unable to cross slip and is given by

$$n_{\alpha 1}(x,y)=\frac{L\rho_\alpha}{4}. \tag{3}$$

A second contribution comes from α-MD's that are able to cross slip towards x. In this case because of the cross slip, only a fraction $e^{-(y-y')/\lambda_\alpha}$ of the MD's that are generated at a point (x,y') will reach the point (x,y). By integrating over the points (x,y') we find a contribution to the MD density

$$n_{\alpha 2}(x,y)=\frac{\lambda_\alpha\rho_\alpha}{2}\left(1-e^{-\frac{L}{2\lambda_\alpha}}\cosh\left(\frac{y}{\lambda_\alpha}\right)\right). \tag{4}$$

Finally β-MD's, which initially glide along the positive or negative x direction and then cross slip towards the y direction, give rise to contributions $n_{\alpha+}(x,y)$ and $n_{\alpha-}(x,y)$, respectively, which are given by

$$n_{\alpha\pm}(x,y)=N\frac{L\rho_\beta}{4}[1-e^{-L/(2\lambda_\beta)}e^{\mp x/\lambda_\beta}]. \tag{5}$$

Here we have taken into account the effect of MD multiplication by the number N of MD's, which are generated on the cross-slip glide plane. An integration has been performed over the region of space from which β-MD's are able to reach to the point (x,y) by $\beta\rightarrow\alpha$ cross slip.

In order to establish a link between the MD densities $n_{\alpha\pm}(x,y)$ and the MD densities that appear in Eq. (1), we note that the latter supposes that the conventional dislocation line direction $\overline{\zeta}$ has been chosen along the positive i direction $(i=x,y)$. It is then worth to note that the direction of the tilt vectors $\overline{b_z}$ x $\overline{\zeta}$ in Fig. 8 is independent of the choice of $\overline{\zeta}$. So if $\overline{\zeta}$ is reversed also $\overline{b_z}$ must change sign. By applying these considerations to the MD's and BV's shown in Fig. 8 we then find that the MD densities $n_{\alpha+}(x,y)$ and $n_{\alpha-}(x,y)$ actually correspond to α-MD's with positive or negative b_z component, respectively. Thus we may calculate the lattice tilt ω_{zy} by directly using these MD densities in Eq. (1). It then follows

$$\omega_{zy}(x,y)=-N\frac{b_zL\rho_\beta}{2}e^{-L/(2\lambda_\beta)}\sinh\left(\frac{x}{\lambda_\beta}\right). \tag{6}$$

In order for this expression to represent a linear variation of the lattice tilts with the x coordinate, we must require that $x\ll\lambda_\beta$ or equivalently $p_i=(L/2)/\lambda_i\ll 1$, where i $=\alpha,\beta$. p_i represents the average cross-slip probability for MD's that glide along the i direction and are able to cross slip. Then Eqs. (4)–(6) can be expanded to first order in the cross-slip probabilities p_α and p_β. In particular, the lattice tilt distribution becomes

$$\omega_{zy}=-b_z\rho_\beta Np_\beta x,$$

$$\omega_{zx}=-b_z\rho_\alpha Np_\alpha y. \tag{7}$$

The needed densities of TD sources ρ_α and ρ_β can be obtained by solving the system of equations

$$\rho_i+\rho_jNp_j=\frac{2n}{L}\quad(i,j=\alpha,\beta;i\neq j). \tag{8}$$

These equations represent the condition of equality between the measured total MD density n and the model prediction of the MD densities $n_i=n_{i1}+n_{i2}+n_{i+}+n_{i-}$ approximated to first order in p_α and p_β. We have here used a single value n for the measured MD density since the measured total densities of α and β-MD's were not very different.[2] We then obtain for the curvatures along the x and y directions

$$\chi_x=\frac{\partial\omega_{zy}}{\partial x}=-\left(\frac{2nb_z}{L}\right)Np_\beta\frac{1-Np_\alpha}{1-N^2p_\alpha p_\beta},$$

$$\chi_y=\frac{\partial\omega_{zx}}{\partial y}=-\left(\frac{2nb_z}{L}\right)Np_\alpha\frac{1-Np_\beta}{1-N^2p_\alpha p_\beta}. \tag{9}$$

VI. DISCUSSION

Equations 6 and 7 indicate that the crucial parameter determining the spatial distribution of lattice tilts is the ratio between the cross-slip glide length and the sample length L/λ. When $\lambda\ll L$, the lattice tilts are limited to regions near the sample border of width $\sim\lambda$ in agreement with the qualitative description of the curvature formation mechanism given by Fig. 9. As λ increases these regions begin to extend over the whole sample length and for $\lambda\gg L$ the lattice tilts vary linearly across the sample as shown by the Eq. (7). Therefore in the framework of our model the buffer layer curvature formation mechanism assumes the aspect of a *''finite sample size effect.''*

The model correctly predicts the main qualitative features of the buffer layer curvature:

(a) the concavity of the curvature: $\partial\omega_{zj}/\partial i<0;(i=x,y;i\neq j)$,

(b) the lattice tilt distribution Eq. (7) satisfies the experimentally observed property $\partial\omega_{zi}/\partial i\approx 0$.

(c) Equation (9) predicts a linear increase of the curvature with the MD density in qualitative agreement with the experimental results shown in Fig. 5.

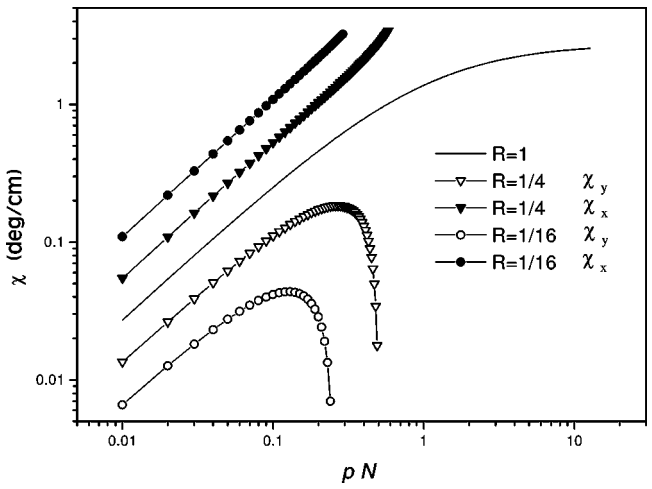

FIG. 10. The model prediction of the buffer layer surface curvature is plotted versus pN, which gives the ratio between dislocations generated by MD multiplication and those generated by other sources. The curvature along the $x=[110]$ and $y=[\bar{1}10]$ directions are shown for different values of the cross-slip asymmetry ratio R.

According to Eq. (9) the curvature asymmetry observed on step-graded buffer layers should be directly related to a difference in the cross-slip probabilities of α and β-MD's. In fact $\chi_x/\chi_y \approx p_\beta/p_\alpha = \lambda_\alpha/\lambda_\beta$. The above observation as well as the form of Eq. (9) suggest to introduce the following change of variables: $R=p_\alpha/p_\beta$ and $p=\sqrt{p_\alpha p_\beta}$.

In Fig. 10 we report the model prediction of the buffer layer surface curvature for a total MD density $n=1.2$ 10^6 cm^{-1} and $L=1.5$ cm. These values represent typical values for our samples. The curvature is shown as a function of pN for different values of the cross-slip asymmetry ratio R. The product pN represents the ratio between the average number of MD's generated by multiplication sources and those generated by other sources. This can be understood by considering that $\rho_j N p_j L/2$ in Eq. (8) gives the density of MD's generated by multiplication, while $\rho_i L/2$ gives the density of MD's generated by extrinsic sources.

For $R=1$ the curvature is symmetric, i.e., $\chi_x=\chi_y$ and reaches the limit value of $(2nb_z)/L=2.7$ deg/cm when $pN \rightarrow \infty$. A comparison between the curve $R=1$ in Fig. 10 and the curvature values in Table I for buffer layers with continuous composition profile suggests that pN lies in the range 0.4–1.5. These values of pN indicate that MD multiplication should be able to produce a fraction of the total MD density that varies in the range from $0.4/(1+0.4)=0.28$ to $1.5/(1+1.5)=0.6$, depending on the composition profile.

In view of the fact that the identification of MD sources in lattice mismatched layers is still largely an open question, and taking into account that MD multiplication has often been proposed as a major source of MD formation, these values appear reasonable to us. For a discussion of MD formation mechanisms in lattice mismatched layers see for instance Refs. 29 and 30.

From the linearity of the lattice tilt distribution in Sec. V, we deduced $p \ll 1$. On the other hand, the above discussion shows that $pN \sim 1$. Therefore we deduce $N \gg 1$. This conclusion is in qualitative agreement with the direct observation of MD pileups in Refs. 9 and 27 in compositionally graded buffer layers where the number of MD's in pileups is found to be of the order of 10.

In the case $R<1$ the curvature is asymmetric and the larger curvature is found for the x direction. Our model indicates that for a given value of pN the larger curvature values should be found for buffer layers with strongly asymmetric curvature. This is in agreeement with the observation of a very large curvature χ_x on the samples ST6 and ST9, which are characterized also by the largest curvature asymmetries.

In Fig. 10 the curvature χ_y decreases to zero at a value $pN=\sqrt{R}$. At the same time the curvature χ_x reaches the limit value of the curvature $(2nb_z)/L$. This behavior can be understood as follows: when $R<1$ more α-MD's are generated by MD multiplication than β-MD's. In particular for $pN \rightarrow \sqrt{R}$ the MD multiplication associated with $\beta \rightarrow \alpha$ cross slip becomes efficient enough to generate all α MD's. Therefore no extrinsic sources are needed to generate α MD's, i.e., $\rho_\alpha \rightarrow 0$. From Eqs. (8) it then follows $\rho_\beta \rightarrow 2n/L=1.6$ 10^6 cm^{-2}, i.e., all β-MD's are generated by extrinsic sources. pN cannot exceed $\sqrt{R}$ since this would imply that more α-MD's are generated than required.

It is interesting to note that the density of extrinsic TD sources $\rho_\beta=1.6$ 10^6 cm^{-2} is higher than the TD densities we observed on our buffer layers, which were typically below 10^5 cm^{-2} (Ref. 2). This indicates that most of the TD's have glided to the sample border during growth, thereby confirming the validity of assumption (ii).

The curvature χ_x on samples ST6 and ST9 is very close to the limit value of the curvature and the curvature χ_y is almost zero. Therefore, according to our model on these samples, almost all of the β-MD's should be generated by extrinsic sources while almost all α-MD's should be generated by MD multiplication. This particular situation is not encountered in continuously graded buffer layers and therefore requires a discussion of the role played by the composition profile in determining the cross slip probability.

In step-graded buffer layers, MD's are confined at several interfaces that are well separated because they are defined by the steplike composition profile. Because in the InGaAs/GaAs system the activation energy for nucleation and glide is lower for α-MD's than for β-MD's, the former are generated first. After α-MD's at the first layer interface have relaxed almost all the strain along the x direction, α-MD's start forming at the second layer interface. Meanwhile the ''slower'' β-MD's still elongate at the first layer interface. Then the gliding TD-arms of β-MD's are subject to strong interactions with α-MD's lying at the second layer interface. This should lead to an enhancement of the pinning probability of TD arms associated with β-MD's and therefore to the preferential activation of Frank-Read and/or spiral multiplication sources related to $\beta \rightarrow \alpha$ cross slip.

On continuously graded buffer layers, MD's are distributed in the volume of the buffer layer instead of being confined to well separated interfaces.[2] All MD's lie below a certain depth and new MD's are always formed at the ''interface'' that separates the dislocation filled region from the dislocation free region close to the surface. Under these conditions α-MD's and β-MD's always form at almost the same depth. As a consequence the preferential formation of

α-MD's should not lead to particularly significant pinning effects and we expect that $\alpha \rightarrow \beta$ and $\beta \rightarrow \alpha$ cross-slip events have comparable probabilities.

Equations (6) to (9) are based on the assumption that the contribution to the MD density from multiple cross slip is negligible compared to that generated in the first multiplication event. Since these contributions can be expected to scale as $(pN)^M$ for M consecutive multiplication events, the validity of the assumption requires relatively small values of the product pN, or equivalently that a relatively small fraction of MD's is generated by MD multiplication. This does not appear to be valid for the case of step-graded buffer layers where we found that almost all α-MD's should be generated by MD multiplication and where the processes of strain relaxation are complicated by a strong dislocation interaction. Therefore, for step-graded buffer layer, the model represents only a first and very rough approximation. Nevertheless the model is able to describe in a qualitatively correct way the basic features of the curvature formation process even in this case. For buffer layers with linear or parabolic composition profile, on the other hand, we found $pN \approx 0.4$ so that the model represents a relatively good aproximation in this case.

VII. CONCLUSIONS

A buffer layer curvature of up to ≈ 3 deg/cm limited to the film region has been observed in compositionally graded InGaAs/GaAs(001) buffer layers and has been related to a linear distribution of the misfit dislocation's Burgers vectors. The origin of this distribution has been explained in terms of a Burgers vector selection occuring in the cross slip of gliding threading dislocations in combination with the long glide length of misfit dislocations in InGaAs/GaAs graded buffer layers. A quantitative model of curvature formation has been presented that describes well the main features of the phenomenon and predicts the right order of magnitude of the buffer layer curvature.

ACKNOWLEDGMENTS

The XRD measurements were conducted at BM05 ESRF within the public user program. We acknowledge S. Gennari, C. Ferrari, and G. Salviati for useful discussions.

*Present address: Laboratoire L2M, CNRS, 196 Avenue Henri Ravera, 92225 Bagneux Cedex, France. Electronic mail: marco.natali@L2M.cnrs.fr

[1] E.A. Fitzgerald, Y.H. Xie, M.L. Green, D. Brasen, A.R. Kortan, J. Michel, Y.-J. Mii, and B.E. Weir, Appl. Phys. Lett. **59**, 811 (1991).

[2] F. Romanato, E. Napolitani, A. Carnera, A.V. Drigo, L. Lazzarini, G. Salviati, C. Ferrari, A. Bosacchi, and S. Franchi, J. Appl. Phys. **86**, 4748 (1999).

[3] F. Romanato, M. Natali, E. Napolitani, A. V. Drigo, A. Bosacchi, C. Ferrari, S. Franchi, and G. Salviati, J. Vac. Sci. Technol. A **16**, 3578 (1998).

[4] J.E. Ayers, S.K. Ghandi, and L.J. Schowalter, J. Cryst. Growth **113**, 430 (1991).

[5] G.H. Olsen and R.T. Smith, Phys. Status Solidi A **31**, 739 (1975).

[6] R.S. Goldman, K.L. Kavanagh, and H.H. Wieder, S.N. Ehrlich, and R.M. Feenstra, J. Appl. Phys. **83**, 5137 (1998).

[7] R.S. Goldman, H.H. Wieder, and K.L. Kavanagh, Appl. Phys. Lett. **67**, 344 (1995).

[8] P.M. Mooney, F.K. LeGoues, J. Tersoff, and J.O. Chu, J. Appl. Phys. **75**, 3968 (1994).

[9] F.K. LeGoues, P.M. Mooney, and J.O. Chu, Appl. Phys. Lett. **62**, 140 (1993).

[10] F.K. Riesz, J. Appl. Phys. **79**, 4111 (1996).

[11] M.D. Lind, G.J. Sullivan, T.Y. Liu, and H. Kroemer, J. Appl. Phys. **64**, 2746 (1988).

[12] J.M. Kang, C.S. Son, Moo-Sung Kim, Yong Kim, Suk-Ki Min, and C.S. Kim, Appl. Phys. Lett. **67**, 641 (1995).

[13] P. Kidd, D.J. Dunstan, H.G. Colson, M.A. Lourenco, A. Sacedon, F. Gonzalez-Sanz, L. Gonzalez, R. Garcia, D. Gonzalez, F.J. Pacheco, and P.J. Goodhew, J. Cryst. Growth **169**, 649 (1996).

[14] J.-I. Chyi, J.-L. Shieh, J.-W. Pan, and R.-M. Lin, J. Appl. Phys. **79**, 8367 (1996).

[15] M. Capano, Phys. Rev. B **45**, 11 768 (1992).

[16] X. Mader, IBM J. Res. Dev. **19**, 151 (1985).

[17] M. Hohnisch, H-J. Herzog, and F. Schaeffler, J. Cryst. Growth **157**, 126 (1995).

[18] C.G. Tuppen, C.J. Gibbing, M. Hockly, and S.G. Roberts, Appl. Phys. Lett. **56**, 54 (1990).

[19] A. Bosacchi, A.C. De Riccardis, P. Frigeri, S. Franchi, C. Ferrari, S. Gennari, L. Lazzarini, L. Nasi, G. Salviati, A.V. Drigo, and F. Romanato, J. Cryst. Growth **175/176**, 1009 (1997).

[20] J.H. Li, G. Bauer, J. Stangl, L. Vanzetti, L. Sorba, and A. Franciosi, J. Appl. Phys. **80**, 81 (1996).

[21] L.C. Feldman, J.W. Mayer, and S.T. Picraux, *Material Analysis by Ion Channeling* (Academic Press, New York 1982).

[22] M. Mazzer, A. Carnera, A. V. Drigo, and C. Ferrari, J. Appl. Phys. **68**, 531 (1990).

[23] C. Ulaq-Bouillet, A. Lefebvre, and J. Di Persio, Philos. Mag. A **69**, 995 (1994).

[24] G. Lacey, C.R. Whitehouse, P.J. Parbrook, A.G. Cullis, A.M. Keir, P. Möck, A.D. Johnson, G.W. Smith, G.F. Clark, B.K. Tanner, T. Martin, B. Lunn, J.H.C. Hogg, M.T. Emeny, B. Murphy, and S. Bennett, Appl. Surf. Sci. **123/124**, 718 (1998).

[25] Z.J. Radzimski, B.L. Jiang, G.A. Rozgonyi, T.P. Humphreys, N. Hamaguchi, and S.M. Bedair, J. Appl. Phys. **64**, 2328 (1988).

[26] J.P. Hirth and J. Lothe, *Theory of Dislocations* (Wiley, New York, 1982).

[27] M.S. Abrahams, J. Blanc, and C.J. Buiocchi, J. Cryst. Growth **21**, 185 (1972).

[28] K.L. Kavanagh, M.A. Capano, L.W. Hobbs, J.C. Barbour, P.M.J. Maree, W. Schaff, J.W. Mayer, D. Pettit, J.M. Wodall, J.A. Stroscio, and R.M. Feenstra, J. Appl. Phys. **64**, 4843 (1988).

[29] R. Beanland, D.J. Dunstan, and P.J. Goodhew, Adv. Phys. **45**, 87 (1996).

[30] *Proceedings of the First International Workshop on Lattice-Mismatched and Heterovalent Thin Film Epitaxy, Barga Italy, 1998*, edited by E.A. Fitzgerald (The Minerals, Metals & Materials Society, Warrendale, 1999).